Advances in Nano Research, *Vol. 18, No. 3 (2025) 205-221*
https://doi.org/10.12989/anr.2025.18.3.205

Stability and vibration analysis of shear deformable FG-CNTRC beams resting on elastic foundations

Kenza Djilali Djebbour[1,2], Mokhtar Nebab[1,3], Mehmet Avcar*[4], Hassen Ait Atmane[1,2], Fabrice Bernard[5], Riadh Bennai[1,2] and Burak İkinci[4]

[1]*Laboratory of Structures, Geotechnics and Risks, Department of Civil Engineering, Hassiba Benbouali University of Chlef, Algeria*
[2]*Department of Civil Engineering, Hassiba Benbouali University of Chlef, Algeria*
[3]*Department of Civil Engineering, Faculty of Technology, University of M'Hamed BOUGARA Boumerdes, Algeria*
[4]*Department of Civil Engineering, Faculty of Engineering and Natural Sciences, Suleyman Demirel University, Cunur, Isparta, Türkiye*
[5]*INSA Rennes, Rennes, France*

(*Received November 7, 2024, Revised February 19, 2025, Accepted February 25, 2025*)

Abstract. This paper presents novel work on the buckling and vibration analysis of shear-deformable functionally graded carbon nanotube-reinforced composite (FG-CNTRC) beams on variable elastic foundations (VEFs). By integrating two-parameter VEF models with a quasi-three-dimensional higher-order shear deformation theory (3D-HSDT). The effective material characteristics of FG-CNTRC beams are described by the rule of mixture. The problem is solved analytically using Navier's technique after the equations of motion are derived using Hamilton's principle. The validity and efficiency of the suggested models and methodology are confirmed by comparing the findings with the results of the available literature. A detailed analysis is conducted on the impact of length-to-thickness ratio, elastic foundation (EF) characteristics, and carbon nanotube (CNT) distribution patterns on the natural frequencies and buckling loads of FG-CNTRC beams, and some benchmark findings are also demonstrated. The results showed that the factors taken into consideration had a significant effect on the FG-CNTRC beams' buckling loads and natural frequencies.

Keywords: beams; buckling load; CNTs; elastic foundation; HSDT; natural frequency

1. Introduction

Carbon nanotubes (CNTs) with one or multiple walls have become a hot topic for numerous scientific and engineering fields due to their exceptional strength, stiffness, and high aspect ratio while having a very low density (Iijima 1991, Thostenson *et al*. 2001, Zhang *et al*. 2020). Owing to its remarkable mechanical and electrical properties, the mechanical behavior of FG-CNTRC has garnered significant attention in recent scientific studies, and so a great deal of research has been done on the analysis of linear and non-linear free vibrations, elastic buckling and post-buckling, and static bending of those structures (Ferreira *et al*. 2005, Bhangale and Ganesan 2006, Shen 2009, Wang and Shen 2012, Lin and Xiang 2014, Tornabene *et al*. 2016, Ghasemi *et al*. 2019, Zerrouki *et al*. 2020, Golmakani *et al* 2021, Nampally *et al*. 2021, Alazwari *et al*. 2022, Cheshmeh *et al*. 2022, Civalek *et al*. 2022, Sobhani and Avcar 2022, Zeighami *et al*. 2023, Abdelrahman *et al*. 2024, Eghbali and Hosseini 2024, Hussain *et al*. 2024, Sekkak *et al*. 2024, Tlidji 2024) investigated the dynamic responses of CNTRC beams using both first-order beam theory (FBT) and third-order beam theory (TBT).

A multi-scale investigation of the CNTRC beams' deflection and stress behavior was provided by Wu *et al*. (2016). For the free vibration analysis of CNTRC beams, Shi *et al*. (2017) proposed a semi-analytical approach based on FSDT and the Fourier method. Mohammadimehr *et al*. (2018) conducted a comparison study of many theories (CPT, TBT, and Reddy's HSDT) to investigate the bending, buckling, and free vibration responses of CNTRC beams. Ranjbar and Feli (2019) conducted an analytical investigation into the low-velocity impact response of micro-cantilever beams composed of axially functionally graded materials using the modified couple stress theory. Babaei *et al*. (2021) examined the thermal buckling and post-buckling of shear deformable FG-CNTRC beams resting on elastic foundations in the framework of different beam models, namely, first-order, third-order, and sinusoidal theories. With reference to the instantaneous fluctuations in martensite volume percentage and, therefore, material nonlinearity along the beam, Fallah *et al*. (2021) explored the non-linear dynamical response of an FG-CNTRC beam with graded shape memory wire. The influence of CNT orientation and gradation distribution, in particular on the static and free vibration analysis of FG-CNTRC beams, was examined by El-Ashmawy and Xu (2021). The concurrent impacts of shear and small scale on the non-linear vibration behavior of FG-CNTRC beams are studied by Taati *et al*. (2022) using the FSDT and nonlocal elasticity theory. Peng *et al*. (2022) studied the influence of boundary relaxation on the free vibration characteristics of FG-CNTRC imperfect beams based on the first-order shear theory.

*Corresponding author, Ph.D.,
E-mail: mehmetavcar@sdu.edu.tr

ISSN: 2287-237X (Print), 2287-2388 (Online)

In order to appropriately fulfil the aims of the applications, the superstructure, foundation, and soil interaction must be taken into consideration in modern structural design and analysis (Hetényi and Hetbenyi 1946, Selvadurai 2013). Therefore, FG-CNTRC structures on EFs have become an open literature interest (Avcar *et al*. 2022, Golmakani and Zeighami 2018, Mellal *et al*. 2024, Nebab *et al*. 2019a, b, c). Yas and Samadi (2012) examined the free vibrations and buckling analysis of nanocomposite beams composed of SWCNTs resting on an EF. Lin and Xiang (2014) developed the eigenvalue equation for the free vibration of aligned CNT composite beams on EF based on the variational principle and first and third-order beam theories. Based on the stretching effect, Khelifa *et al*. (2018) examined the buckling of CNTRC beams resting on an EF. Using Timoshenko beam theory (TBT), Mohseni and Shakouri (2019) examined the free vibration and buckling of FG-CNTRC beams with varying thicknesses resting on EFs. Ghorbani *et al*. (2019) introduced a higher-order beam theory for free vibration and buckling of CNTRC micro beams embedded in EFs using the stress-strain gradient framework. Dynamic study of a FG-CNTRC beam resting on a viscoelastic foundation was studied by Kiarasi *et al*. (2022). Based on a higher-order shear deformation theory, Yuan *et al*. (2023) investigated the vibration analysis of viscoelastic nanobeams reinforced by FG-CNTs, taking into account the thickness stretching effect exposed to magneto-hygro-thermal loading.

Other recent research work has focused on improving the mechanical properties of advanced composite structures, particularly those reinforced with functional gradient carbon nanotubes (FG-CNTRC). Beitollahi *et al*. (2025) explored the effect of variable length scaling parameter on the agglomeration of nanoparticles in nanocomposites, thus influencing their overall mechanical behaviour. In addition, Gawah *et al*. (2025) studied the bending of FG plates reinforced with graphene wafers resting on Kerr-type foundations, using a higher-order shear deformation theory. Zhang *et al*. (2023) analysed wave propagation in CNTRC beams resting on elastic foundations, comparing different higher-order beam theories. In addition, Youzera *et al*. (2025) evaluated the free vibration of cylindrical sandwich hulls with FG-CNTRC composite facings using the differential quadrature (DQ) method. Alsubaie *et al* (2024) demonstrated the impact of porosity distributions on the buckling and bending of FG-CNTRC composite beams, while Cuong *et al*. (2024) developed finite element modelling to predict the static bending response of rotating FG-CNTRC beams subjected to complex thermal conditions. Finally, a complementary study proposed by Alsubaie *et al*. (2023) to examine the influence of porosity on the vibrations of FG-CNTRC composite beams, highlighting the importance of microstructural characteristics on the dynamics of composite structures.

The growing interest in FG-CNTRC beams stems from their exceptional mechanical properties and adaptability in advanced engineering applications. However, research on their stability and vibration behavior on variable elastic foundations using quasi-3D-HSDT remains limited. This study addresses this gap by investigating the effects of CNT distribution, foundation parameters, and geometric ratios on their dynamic performance. While various beam theories have been applied to study FG-CNTRC beams with and without elastic foundations (EFs), the analysis of such beams on variable two-parameter elastic foundations using quasi-3D-HSDT has not yet been explored.

Elastic foundation models, such as the Winkler, Pasternak, and Kerr models, have evolved to better represent soil-structure interaction. The Winkler model, the simplest, uses independent linear springs, while the Pasternak model incorporates shear interaction, and the Kerr model introduces a two-layer spring system for enhanced realism. Studying variable foundations is essential because real-world soil conditions are often non-uniform, significantly influencing the structural response of beams and plates. Accurate modeling of these variations is critical for predicting stability, vibration, and load-bearing capacity, ensuring the safe and efficient design of structures on elastic foundations.

Consequently, this research resides in its comprehensive approach to analysing the dynamic response of FG-CNTRC beams taking into account variable elastic foundations, which has not been fully explored in previous studies. In order to do this, the current study examines the free vibration and buckling characteristics of FG-CNTRC beams on VEFs employing quasi-3D-HSDT. The rule of mixture is utilized to describe the effective material properties of FG-CNTRC beams. Four different CNT distribution patterns (FG-X, FG-O, FG-V, and UD) are considered in this context. Besides, an alternative formula for beam reinforcement (n-FG-X), showing the non-linear distribution patterns of CNTs is also considered. Hamilton's principle is used to derive the equations of motion, while Navier's method is used to solve the problem analytically. The effects of carbon CNT distribution patterns, elastic EF parameters, and length-to-thickness ratio on the natural frequencies and buckling loads of shear deformable FG-CNTRC beams are examined in detail. Employing the quasi-3D higher-order shear deformation theory (HSDT) model in conjunction with the two-parameter variable elastic foundation (VEF) model yields a more refined analytical framework for characterizing the mechanical behavior of these composite beams. The findings of this study offer critical insights that enhance our understanding of FG-CNTRC beam performance and support the design and optimization of such systems in engineering applications, including aerospace, civil, and mechanical structures, where both stiffness and dynamic response are of paramount importance.

2. The formulation of the problem

2.1 The material characteristics

Fig. 1 shows the five types of the FG-CNTRC beam on the EFs, i.e., uniform (UD) and distribution patterns across the thickness of the beam thickness, designated as FG-V, FG-O, FG-X, and n-FG-X, with the length (L), width (b), and thickness (h). The volume fraction (V_{CNT}^{*}) remains

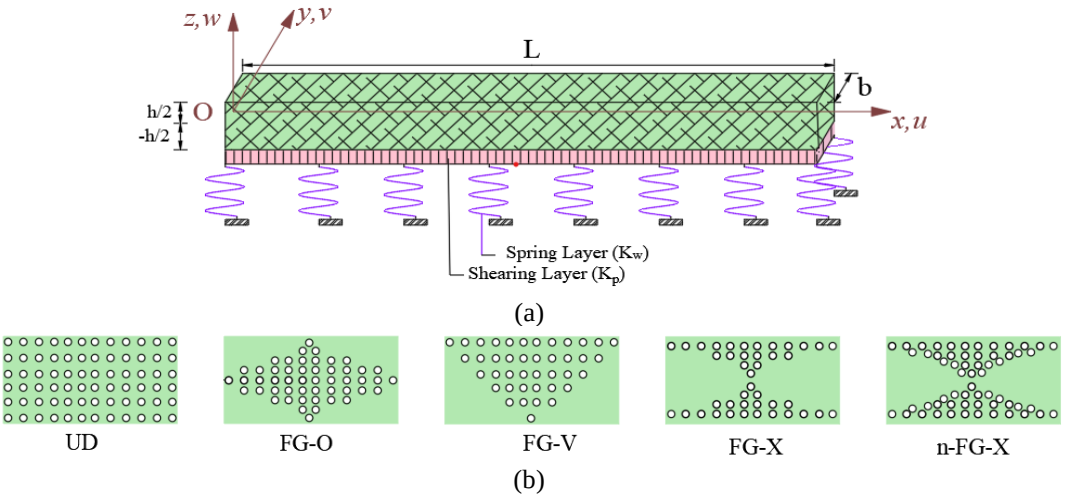

Fig. 1 a) The geometry and b) CNT configurations of FG-CNTRC beam on EFs

constant throughout all combinations. Here, the FG-CNTRC beam is enriched evenly with CNTs in UD; the upper surface of the beam is enriched with CNTs, while the lower surface is CNT-free in the FG-V configuration; the top and bottom surfaces are CNT-free in FG-O design while the top and bottom surfaces are enriched with CNTs in the FG-X configuration (Golmakani and Zeighami 2018).

By using the rule of mixture, the effective Young's and shear modulus of FG-CNTRC beams can be computed as follows (Golmakani *et al*. 2021):

$$E_{11} = \eta_1 V_{cnt} E_{11}^{cnt} + V_m E^m \tag{1a}$$

$$\frac{\eta_2}{E_{22}} = \frac{V_m}{E^m} + \frac{V_{cnt}}{E_{22}^{cnt}} \tag{1b}$$

$$\frac{\eta_3}{G_{12}} = \frac{V_m}{G^m} + \frac{V_{cnt}}{G_{12}^{cnt}} \tag{1c}$$

where E_{11}^{cnt}, E_{22}^{cnt} and G_{12}^{cnt} indicate Young's modulus and shear modulus of CNTs, respectively, E^m and G^m represent the similar characteristics of the isotropic matrix, V_{cnt} and V_m are the volume fractions of the carbon nanotube and the matrix, which are connected by the following formula

$$V_m + V_c = 1 \tag{2}$$

The mass density (ρ) and Poisson's ratio (ν) of the FG-CNTRC beams can be represented similarly as Yas and Samadi (2012):

$$\nu(z) = V_{cnt}\nu^{cnt} + V_m\nu^m \tag{3}$$

$$\rho(z) = V_m\rho^m + V_{cnt}\rho^{cnt} \tag{4}$$

where ν^{cnt}, ν^m are the Poisson's ratios, and ρ^{cnt}, ρ^m are the densities of CNTs and matrix, respectively.

The variations of the volume fractions of CNTs along the thickness direction of the CNTRC beams for different configurations are as follows (Yas and Samadi 2012):

$$\text{UD: } V_{cnt} = V_{cnt}^* \tag{5}$$

$$\text{FG-V: } V_{cnt} = (1 + \frac{2z}{h})V_{cnt}^* \tag{6}$$

$$\text{FG-X: } V_{cnt} = 4\frac{|z|}{h}V_{cnt}^* \tag{7}$$

$$\text{FG-O: } V_{cnt} = 2 - 4\frac{|z|}{h}V_{cnt}^* \tag{8}$$

Furthermore, in the current study, another formulation is also used to characterize the variation in CNT distribution patterns across the thickness of a beam. This formulation incorporates a non-linear distribution pattern of CNTs throughout the beam cross-section, with an index parameter (denoted as "n") capturing the nonlinearity inherent in CNTs (Avcar *et al*. 2023):

$$\text{n-FG-X: } V_{cnt} = (n+1)\left(2 \times \frac{|z|}{h}\right)^n V_{cnt}^* \tag{9}$$

The specified volume fraction of CNTs (V_{CNT}^*) can be established by:

$$V_{cnt}{}^* = \frac{H_{CNT}}{H_{CNT} + \frac{\rho_{CNT}}{\rho_m} - \frac{\rho_{CNT}}{\rho_m}H_{CNT}} \tag{10}$$

In this case, ρ^m, ρ^{cnt}, and W_{cnt} represent the mass densities of the matrix and CNTs and the mass fraction of CNTs, respectively.

2.2 Two parameter variable elastic foundations

A two-parameter VEF supports the FG-CNTRC beam with enhanced characteristics. The first layer consists of Winkler springs without coupling effects, while the second layer includes a shear layer of Pasternak that joins the Winkler springs. The following thorough formulation establishes the features of the EFs using the Winkler-Pasternak model (Nebab *et al*. 2019a, b, c):

$$f_e(x) = K_w(x)w - K_p\left(\frac{\partial^2 w}{\partial x^2}\right) \tag{11}$$

where f_e is the response of the EF, $K_w(x)$ is the parameter regarding the variable Winkler EF, and K_p is the constant regarding the Pasternak layer.

The formulation regarding the variable Winkler EF is described as follows (Nebab *et al*. 2019a, b, c):

$$K_w(x) = \frac{k_w}{L^2}\begin{cases} 1+\Psi\left(\frac{x}{L}\right) & \text{Linear} \\ 1+\Psi\left(\frac{x}{L}\right)^2 & \text{Parabolic} \\ 1+\Psi\left(sin\left(\pi\frac{x}{L}\right)\right) & \text{Sinusoidal} \\ 1+\Psi\left(cos\left(\pi\frac{x}{2L}\right)\right) & \text{Cosine} \\ 1+\Psi\left(exp\left(\frac{x}{L}\right)-exp\left(\frac{x}{L}\right)^n\right) & \text{Exponential} \end{cases} \quad (12)$$

where, k_w and Ψ are constant and VEF parameters. Note that if Ψ is zero, the EF becomes uniform.

2.3 Equations of motion

Higher-order shear deformation theories (HSDTs) provide significant advantages over classical theories, such as Euler-Bernoulli or Timoshenko beam theories, by delivering a more accurate representation of shear deformation and stress distribution, particularly in thick or composite structures, while accounting for warping effects. By definition, the displacements along the x- and z-axes of every point in the FG-CNTRC beam are denoted as u (x, z, t) and w (x, z, t), respectively, in the framework of higher-order shear deformable beam theory (Mellal *et al*. 2022):

$$u(x,z,t) = u_0(x,t) - z\frac{\partial w_0(x,t)}{\partial x} + k_1 f(z)\int \theta(x,t)dx \quad (13a)$$

$$w(x,z,t) = w_0(x,t) + g(z)\phi_z(x,t) \quad (13b)$$

The proposed hypothesis of the present research aims to accomplish the following (Nebab *et al*. 2019a):

$$f(z) = \frac{2}{3\pi}\left(z\,cosh\left(\frac{\pi}{2}\right) - h\,sinh\left(\frac{z\pi}{h}\right)\right) \quad (14a)$$

$$g(z) = \frac{\partial f(z)}{\partial z} \quad (14b)$$

The strains associated with the displacements are as follows:

$$\{\varepsilon_x\} = \{\varepsilon_x^0\} + z\{k_x^b\} + f(z)\{k_x^s\} \quad (15a)$$

$$\{\gamma_{xz}\} = g(z)\{\gamma_{xz}^0\} \quad (15b)$$

$$\varepsilon_z = g'(z)\varepsilon_z^0 \quad (15c)$$

where the following definitions apply

$$(\varepsilon_x^0) = \left(\frac{\partial u_0}{\partial x}\right), \quad (k_x^b) = \left(-\frac{\partial^2 w}{\partial^2 x}\right), \quad (k_x^s) = (k_1\theta), \quad (16a)$$

$$\{\gamma_{xz}^0\} = \left\{k_1\int\theta dx + \frac{\partial\phi_z}{\partial x}\right\}, \quad (16b)$$

$$\varepsilon_z^0 = \phi_z \quad (16c)$$

$$g'(z) = \frac{\partial g(z)}{\partial z} \quad (16d)$$

The undefined integral in the strains relation may be simplified and rebuilt as follows by using Navier methods on the format derivation:

$$\int \theta dx = A'\frac{\partial\theta}{\partial x} \quad (17)$$

where the coefficients denoted as A' are determined using the Navier method. Thus, the values of A' and k_1 can be defined as follows:

$$A' = -\frac{1}{\alpha^2},\ k_1 = \alpha^2 \quad (18a)$$

$$\alpha = \frac{n\pi}{L} \quad (18b)$$

The following are the stress-strain relationships of the FG-CNTRC beam as determined by Hooke's law:

$$\begin{Bmatrix}\sigma_x\\ \sigma_z\\ \tau_{xz}\end{Bmatrix} = \begin{bmatrix}Q_{11} & Q_{13} & 0\\ Q_{13} & Q_{33} & 0\\ 0 & 0 & Q_{44}\end{bmatrix}\begin{Bmatrix}\varepsilon_x\\ \varepsilon_z\\ \gamma_{xz}\end{Bmatrix} \quad (19)$$

where $(\sigma_x, \sigma_z, \tau_{xz})$ and $(\varepsilon_x, \varepsilon_z, \gamma_{xz})$ are the stress and strain components, respectively.

The stiffness coefficients for the 2D Higher-Order Shear Deformation Theory (2D-HSDT) and the quasi-3D HSDT theory can be expressed as follows:

$$\text{2D-HSDT: } Q_{11} = E(z), Q_{33} = 0, \quad Q_{44} = G_{12}\ , Q_{13} = Q_{31} = 0 \quad (14a)$$

$$\text{quasi-3D HSDT: } Q_{11} = Q_{33} = \frac{E(z)}{(1-\nu^2)},\ Q_{44} = G_{12}, \quad Q_{13} = Q_{31} = \frac{\nu E(z)}{(1-\nu^2)} \quad (14b)$$

Note that throughout out the thickness, the modulus $E, G,$ and the elastic coefficients Q_{ij} vary.

The following is how Hamilton's principle is used to construct the equations of motion (Belarbi *et al*. 2023):

$$\int_0^t (\delta U + \delta U_{ef} - \delta K)\ dt = 0 \quad (21)$$

where δ denotes a variation, and U, U_{ef} and K stand for the strain energy of the FG-CNTRC beam, the strain energy of EFs, and the kinetic energy, respectively.

An expression regarding the FG-CNTRC beam's strain energy variations is as follows:

$$\delta U = \int_V (\sigma_{xx}\delta\varepsilon_{xx} + \sigma_{zz}\delta\varepsilon_{zz} + \tau_{xz}\delta\gamma_{xz})\text{dV} = \int_A (N_x\delta\varepsilon_x^0 + +N_z\delta\varepsilon_z^0 + M_x^b\delta k_x^b + M_x^s\delta k_x^s + R_{xz}^s\delta R_{xz}^s)\ \text{dA} \quad (22)$$

where N_i^i, M_i^i and R_i^i are the stress resultants, which are described as follows:

$$(N_x, M_x^b, M_x^s) = \int_{-\frac{h}{2}}^{\frac{h}{2}} (\sigma_x, \tau_{xy})(1, z, f(z))\, dz, \quad (23a)$$

$$N_z = \int_{-h/2}^{h/2} (\sigma_z) g'(z) \quad dz \quad (23b)$$

$$(R_{xz}^s) = \int_{-h/2}^{h/2} (\tau_{xz}) g(z) dz \quad (23c)$$

Based on higher-order shear deformation theory, the variation of kinetic energy may be expressed as follows:

$$\delta K = \int_V \rho(z)(\dot{u}\delta\dot{u} + \dot{w}\delta\dot{w})\, dV$$

$$= \int_A \left\{ \begin{array}{c} I_0(\dot{u}_0\delta\dot{u}_0 + \dot{w}_0\delta\dot{w}_0) \\ -I_1\left(\dot{u}_0\dfrac{\partial\delta\dot{w}_0}{\partial x} + \dfrac{\partial\dot{w}_0}{\partial x}\delta\dot{u}_0\right) \\ +J_1\left((k_1A')\left(\dot{u}_0\dfrac{\partial\delta\dot{\theta}}{\partial x} + \dfrac{\partial\dot{\theta}}{\partial x}\delta\dot{u}_0\right)\right) \\ +I_2\left(\dfrac{\partial\dot{w}_0}{\partial x}\dfrac{\partial\delta\dot{w}_0}{\partial x}\right) \\ +K_2\left((k_1A')^2\left(\dfrac{\partial\dot{\theta}}{\partial x}\dfrac{\partial\delta\dot{\theta}}{\partial x}\right)\right) \\ -J_2\left((k_1A')\left(\dfrac{\partial\dot{w}}{\partial x}\dfrac{\partial\delta\dot{\theta}}{\partial x} + \dfrac{\partial\delta\dot{w}}{\partial x}\dfrac{\partial\dot{\theta}}{\partial x}\right)\right) \\ +J_0(\dot{\phi}_z\delta\dot{w}_0 + \dot{w}_0\delta\dot{\phi}_z) + K_3(\dot{\phi}_z\delta\dot{\phi}_z) \end{array} \right\} dA \quad (24)$$

where the differentiation with respect to the time variable t is indicated by the dot-exponent and the following equations define the mass moment of inertias:

$$\begin{aligned} &(I_0, I_1, I_2) = \int_{-h/2}^{h/2} (1, z, z^2)\rho(z)dz \\ &(J_0, J_1, J_2, K_2, K_3) \\ &= \int_{-h/2}^{h/2} (g, f(z), z \quad f(z), f(z)^2, g(z)^2)\rho(z)dz \end{aligned} \quad (25)$$

The change in the deformation energy of EFs with varying characteristics may be written as

$$\delta U_{ef} = \int_A -K_P\left(\frac{d^2w_0}{dx^2} + \frac{d^2w_0}{dy^2}\right)\delta w_0)\, dA \quad (26)$$

The equations of motion for the FG-CNTRC beam can be derived by substituting the expressions for δU, δK, and δU_{ef} from Eqs. (22), (24), and (26) into Eq. (21) and collecting the coefficients of δu_0, δw_0 and $\delta\varphi$ while carrying out integration by parts:

$$\delta u_0: \quad \frac{\partial N_x}{\partial x} = I_0\ddot{u}_0 - I_1\frac{\partial\ddot{w}_0}{\partial x} + J_1 k_1A'\frac{\partial\ddot{\theta}}{\partial x} \quad (27a)$$

$$\delta w_0: \quad \frac{\partial^2 M_x^b}{\partial x^2} + K_w w_0 - K_P\left(\frac{d^2w_0}{dx^2}\right) = J_0\ddot{\phi} - I_0\ddot{w}_0 + I_1\left(\frac{\partial\ddot{u}_0}{\partial x}\right) - I_2\nabla^2\ddot{w}_0 + J_2\left(k_1A'\frac{\partial^2\ddot{\theta}}{\partial x^2}\right) \quad (27b)$$

$$\delta\theta: \quad -k_1M_x^s + k_1A'\frac{\partial R_{xz}^S}{\partial x} = -J_1\left(k_1A'\frac{\partial\ddot{u}_0}{\partial x} + \right) - K_2\left((k_1A')^2\frac{\partial^2\ddot{\theta}}{\partial x^2}\right) + J_2\left(k_1A'\frac{\partial^2\ddot{w}}{\partial x^2}\right) \quad (27c)$$

$$\delta\phi_z: \frac{\partial R_{xz}^S}{\partial x} - N_z = J_0\ddot{w}_0 + K_3\ddot{\phi} \quad (27d)$$

By substituting Eq. (15) into Eq. (19) and integrating across the thickness of the FG-CNTRC beam, the stress resultants are expressed as:

$$\begin{bmatrix} N_x \\ M_x^b \\ M_x^s \\ N_z \end{bmatrix} = \begin{bmatrix} A_{11} & B_{11} & B_{11}^s & X_{13} \\ B_{11} & D_{11} & D_{11}^s & Y_{13} \\ B_{11}^s & D_{11}^s & H_{11}^s & Y_{13}^s \\ X_{13} & Y_{13} & Y_{13}^s & Z_{33} \end{bmatrix} \begin{bmatrix} \dfrac{\delta u_0}{\delta x} \\ \dfrac{\delta^2\omega_0}{\delta x^2} \\ k\theta \\ \varphi_z \end{bmatrix} \quad (28)$$

$$\{R_{xz}^s\} = [A_{55}^s]\left\{k_1A'\frac{\partial\theta}{\partial x} + \frac{\partial\phi_z}{\partial x}\right\} \quad (29)$$

where, and stiffness components are defined as follows:

$$(A_{ii}, B_{ii}, D_{ii}, B_{ii}^s, D_{ii}^s, H_{ii}^s) = \int_{-h/2}^{h/2} Q_{ij}(1, z, z^2, f(z), zf(z), f^2(z))dz, \ (i = 1) \quad (30a)$$

$$(X_{ij}, Y_{ij}, Y_{ij}^s, Z_{ii}) = \int_{-h/2}^{h/2} Q_{ij}(1, z, f(z), g'(z))g'(z)dz, \ (i, j = 1,3) \quad (30b)$$

$$A_{ij}^s = \int_{-h/2}^{h/2} Q_{44}[g(z)]^2 dz, \ (i, j = 4) \quad (30c)$$

Consequently, the equations of motion for FG-CNTRC beams on EFs can be expressed in terms of displacements (δu_0, δw_0, $\delta\theta$, $\delta\varphi$) as follows:

$$\begin{aligned} &A_{11}d_{11}u_0 - B_{11}d_{111}w_0 + (B_{11}^s k_1)d_1\theta - X_{13}d_1\phi_z \\ &= I_0\ddot{u}_0 - I_1d_1\ddot{w}_0 + J_2A'k_1d_1\ddot{\theta} \end{aligned} \quad (31a)$$

$$\begin{aligned} &B_{11}d_{111}u_0 - D_{11}d_{1111}w_0 + (D_{11}^s k_1)d_{11}\theta \\ &+K_w(x)w_0 - K_p(\frac{d^2w_0}{dx^2}) + Y_{13}d_{11}\phi_w = \\ &I_0\ddot{w}_0 + J_0\ddot{\phi}_z + I_1(d_1\ddot{u}_0) - I_2(d_{11}\ddot{w}_0) + J_2k_1A'd_{11}\ddot{\theta} \end{aligned} \quad (31b)$$

$$\begin{aligned} &-(B_{11}^s k_1)d_1u_0 + (D_{11}^s k_1)d_{11}w_0 - H_{11}^s k_1^2\theta \\ &+A_{55}^s(k_1A')^2d_{11}\theta - k_1Y_{13}^s\phi_z + A_{55}^s(k_1A')^2d_{11}\phi_z \\ &= -J_1(k_1A'd_1\ddot{u}_0) + J_2(k_1A'd_{11}\ddot{w}_0) \end{aligned} \quad (31c)$$

$$\begin{aligned} &-X_{13}d_1u_0 + (Y_{13}d_{11})w_0 + (A_{44}^s k_1A'^{d_{11}} - Y_{13}^s k_1)\theta \\ &+(A_{44}^s d_{11} - Z_{33})\phi_z = J_0\ddot{w}_0 + K_3 + \ddot{\phi}_z \end{aligned} \quad (31d)$$

where d_{ij}, d_{ijl} and d_{ijlm} consist of the subsequent differential operators:

$$d_{ij} = \frac{\partial^2}{\partial x_i \partial x_j}, \quad d_{ijl} = \frac{\partial^3}{\partial x_i \partial x_j \partial x_l},$$
$$d_{ijlm} = \frac{\partial^4}{\partial x_i \partial x_j \partial x_l \partial x_m}, \quad (32)$$
$$d_i = \frac{\partial}{\partial x_i}, (i,j,l,m = 1,2).$$

3. Analytical solution of the problem

Since the FG-CNTRC beam on EFs is supposed to have simply supported edges, the governing differential equation of the current problem is solved using Navier's method. For this context, the following expressions regarding the variables u_0, w_0, θ_0, and ϕ_z are employed to achieve this goal:

$$\begin{Bmatrix} u_0 \\ w_0 \\ \theta \\ \phi_z \end{Bmatrix} = \sum_{m=1}^{\infty} \begin{Bmatrix} U_m\, cos(\alpha\, x) e^{i\omega_m t} \\ W_m\, sin(\alpha\, x) e^{i\omega_m t} \\ X_m\, sin(\alpha\, x) e^{i\omega_m t} \\ Y_m\, sin(\alpha\, x) e^{i\omega_m t} \end{Bmatrix} \quad (33)$$

where, U_m, W_m, X_m, and $Y_m$are random unknown values which are needed to be determined, and ω is the eigen frequency linked to the eigenmode (m), and $\alpha = m\pi/L$. The following eigenvalue equations can be obtained for any fixed value of n by inserting Eq. (33) into the Eq. (31), which accounts for the free vibration of FG-CNTRC beams on VEFs:

$$\left(\begin{bmatrix} S_{11} & S_{12} & S_{13} & S_{14} \\ S_{21} & S_{22} & S_{23} & S_{24} \\ S_{31} & S_{32} & S_{33} & S_{34} \\ S_{41} & S_{42} & S_{43} & S_{44} \end{bmatrix} - \omega^2 \begin{bmatrix} m_{11} & m_{12} & m_{13} & m_{14} \\ m_{21} & m_{22} & m_{23} & m_{24} \\ m_{31} & m_{32} & m_{33} & m_{34} \\ m_{41} & m_{42} & m_{43} & m_{44} \end{bmatrix} \right) \begin{Bmatrix} U_n \\ W_n \\ \theta_n \\ \varphi_n \end{Bmatrix} = \begin{Bmatrix} 0 \\ 0 \\ 0 \\ 0 \end{Bmatrix} \quad (34a)$$

Also, the next equation is derived for the buckling analysis of FG-CNTRC beams on VEFs:

$$\left(\begin{bmatrix} S_{11} & S_{12} & S_{13} & S_{14} \\ S_{21} & S_{22} & S_{23} & S_{24} \\ S_{31} & S_{32} & S_{33} & S_{34} \\ S_{41} & S_{42} & S_{43} & S_{44} \end{bmatrix} - \Lambda \begin{bmatrix} 0 & 0 & 0 & 0 \\ 0 & 0 & \beta & 0 \\ 0 & 0 & 0 & 0 \\ 0 & 0 & 0 & 0 \end{bmatrix} \right) \begin{Bmatrix} U_n \\ W_n \\ \theta_n \\ \varphi_n \end{Bmatrix} = \begin{Bmatrix} 0 \\ 0 \\ 0 \\ 0 \end{Bmatrix} \quad (34b)$$

where

Table 1 The efficiency parameters of CNTs

V_{cnt}^*	η_1	$\eta_2 = \eta_3$
0.12	1.2833	1.0566
0.17	1.3414	1.7101
0.28	1.3238	1.7380

$$\begin{aligned} &S_{11} = -(A_{11}\alpha^2), \quad S_{12} = S_{21} = \alpha B_{11}\alpha^2, \\ &S_{13} = S_{31} = \alpha B_{11}^s k, \quad S_{14} = S_{41} = \alpha X_{13}, \\ &S_{22} = -D_{11}\alpha^2 - k_p\alpha^2, \; S_{23} = -k_1 D_{11}^s \alpha^2, \\ &S_{24} = (\alpha^2 Y_{13}), \; S_{33} = (-k_1 H_{11}^s k_1 - (k_1 k_p)^2 A_{44}^s \alpha^2), \\ &S_{44} = (-\alpha^2 A_{44}^s - Z_{33}), \\ &S_{43} = (-k_1 Y_{13}^s - \alpha^2 k_1 A' A_{44}^s) \end{aligned} \quad (35)$$

$$\begin{aligned} &m_{11} = -I_0, \quad m_{12} = m_{21} = \alpha_1 I_1, \\ &m_{13} = m_{31} = -J_1 k_1 A' \alpha, \quad m_{14} = m_{41} = 0, \\ &m_{22} = (-I_0 - I_2\alpha^2), \quad m_{23} = (-J_2 k_1 A' \alpha^2), \\ &m_{24} = J_0, \quad m_{33} = (-K_2 (k_1 A')^2 \alpha^2, \\ &m_{34} = m_{43} = 0, \quad m_{44} = -K_3, \quad \beta = Ncr\alpha^2 \end{aligned} \quad (36)$$

4. Numerical results and discussion

A detailed examination of the numerical findings pertaining to the buckling and vibration of FG-CNTRC beams is given in this section. In this study, size-dependent properties of the FG-CNTRC beam are captured using the three efficiency parameters given in Table 1, which are related to the volume fraction and offered by Yas and Samadi (2012) depending on molecular dynamic simulations of Han and Elliott (2007). Furthermore, the matrix is assumed to be made of polymethyl methacrylate (PMMA), with the material properties: $\nu^p = 0.3$; $\rho^p = 1190 kg/m^3$ and $E^p = 2.5GPa$; as well as the armchair (10, 10) SWCNTs are assumed to be used as reinforcing material with the properties: $\nu^{cnt} = 0.19$; $\rho^{cnt} = 1400 kg/m^3$; $E_{11}^{cnt} = 600GPa$; $E_{22}^{cnt} = 10GPa$ and $G_{12}^{cnt} = 17.2GPa$ (Yas and Samadi 2012).

The natural frequency and critical buckling load are represented by the dimensionless parameters shown below for ease of usage and comparisons, respectively:

$$\text{NDNF: } \varpi = \omega L \sqrt{\frac{I_{10}}{A_{110}}} \quad (37)$$

$$\text{NDCBL: } \bar{N} = \frac{N_x^0}{A_{110}} \quad (38)$$

where A_{110} and I_{10} are the same values as A_{11} and I_0 of the beam made of pure matrix material, respectively; and N_x^0 is critical buckling load.

4.1 Verification examples

Example 1: Table 2 presents results regarding non-dimensional fundamental natural frequencies (NDFNFs) ($\varpi = \sqrt{(\rho_c h L^4 \omega^2 / EI)}$) of the isotropic homogenous beams on EFs employing Quasi-3D HSDT are compared with

Table 2 Comparisons of the NDFNFs of an isotropic homogeneous beam on EFs

L/h=120					
k_w	k_P	(Ying *et al*. 2008)	(Chen *et al*. 2004)	(Ait Atmane *et al*. 2017)	Present
0	0	3.14145	3.14143	3.14214	3.14213
	1	3.73587	3.73588	3.73629	3.73628
	2.5	4.29689	4.29687	4.29716	4.29715
10^2	0	3.74823	3.74823	3.74864	3.74864
	1	4.14357	4.14356	4.14388	4.14387
	2.5	4.58227	4.58227	4.58249	4.58249
10^4	0	10.02403	10.02403	10.02405	10.02405
	1	10.04812	10.04813	10.04814	10.04814
	2.5	10.08393	10.08394	10.08395	10.08395
L/h=15					
k_w	k_p	(Ying *et al*. 2008)	(Chen *et al*. 2004)	(Ait Atmane *et al*. 2017)	Present
0	0	3.13227	3.13025	3.13093	3.13081
	1	3.72775	3.72657	3.727	3.72686
	2.5	4.28886	4.28809	4.28845	4.28829
10^2	0	3.74012	3.73895	3.73937	3.73923
	1	4.13558	4.13472	4.13508	4.13493
	2.5	4.5741	4.57347	4.57383	4.57366
10^4	0	9.99583	9.99582	10.00663	10.00636
	1	10.01971	10.0197	10.03065	10.03038
	2.5	10.0552	10.05519	10.06635	10.06608
L/h=5					
k_w	k_p	(Ying *et al*. 2008)	(Chen *et al*. 2004)	(Ait Atmane *et al*. 2017)	Present
0	0	3.06373	3.04799	3.04842	3.0404
	1	3.66645	3.65802	3.65989	3.65047
	2.5	4.22319	4.21834	4.22492	4.21442
10^2	0	3.67882	3.6705	3.67243	3.66299
	1	4.072	4.06636	4.07127	4.06104
	2.5	4.50278	4.49914	4.50972	4.49878
10^4	0	7.34081	7.34081	7.55257	7.55257
	1	7.34095	7.34095	7.55257	7.55257
	2.5	7.34116	7.34116	7.55257	7.55257

those of Chen *et al*. (2004), Ying *et al*. (2008), and Ait Atmane *et al*. (2017) using different beam theories versus length-to-thickness ratio (*L/h*) and foundation parameters, k_w and k_p. Thus, it is seen that the obtained results are in good agreement with the previously published ones, while the small discrepancies seem to arise from the adopted theory.

Example 2: In Table 3, present results regarding non-dimensional fundamental natural frequencies (NDFNFs) ($\varpi = \sqrt{(\rho_c h L^4 \omega^2 / EI)}$) of the FG beams are compared with those of Mellal *et al*. (2023) versus different *L/h* and VEFs. The material properties utilized in this example are obtained from the investigation conducted by Mellal *et al*. (2024). This comparison aims to confirm the effectiveness of the used approach. The characteristics of the FG material are integrated into the program by substituting the FG-CNTRC properties with those of Al/Al_2O_3 in the material declaration section. Thus, it is seen that the present results are in good agreement with the previously published ones, while minor discrepancies seem to arise from the adopted beam theory.

Example 3: Table 4 presents the effects of the EF coefficients and the various values of the CNT volume fraction on the first three NDNFs of FG-CNTRC for *L/h*=15. The results obtained are also compared with those of Yas and Samadi (2012). Note that (k_w, k_p) = (0.1, 0.02) indicates the Pasternak EF; (k_w, k_p) = (0.1, 0) indicates the Winkler EF, and (k_w, k_p) = (0, 0) indicates the foundationless case. The values of NDNFs increase as a function of the k_w, k_p, respectively, as well as when the V^*_{CNT} increases. The lowest NDNFs are observed in the FG-O configuration, which appears authentic due to the lower density of CNTs. Remarkably, FG-X consistently yields the

Table 3 Comparisons of the NDFNFs of an FG beam on EFs

L/h	p	Foundation type									
		linear		parabolic		sin		exp		cos	
		(Mellal *et al*. 2023)	Present	(Mellal *et al*. 2023)	Present	(Mellal *et al*. 2023)	Present	(Mellal *et al*. 2023)	Present	(Mellal *et al*. 2023)	Present
5	0	5.0753	5.0380	4.1008	4.0777	5.3725	5.3303	4.9044	4.8697	5.2342	5.1943
	1	5.2067	5.1704	4.1079	4.0875	5.5295	5.4879	5.0191	4.9858	5.3798	5.3407
	2	5.2638	5.2297	4.1290	4.1090	5.5918	5.5546	5.0719	5.0400	5.4401	5.4041
	5	5.3338	5.2987	4.1728	4.1477	5.6522	5.6283	5.1403	5.1053	5.5082	5.4761
	8	5.3603	5.3232	4.1909	4.1622	5.6508	5.6524	5.1675	5.1287	5.5287	5.5010
	10	5.3702	5.3321	4.1971	4.1669	5.6327	5.6600	5.1779	5.1371	5.5330	5.5100
20	0	5.1231	5.1219	4.1561	4.1556	5.4199	5.4186	4.9527	4.9516	5.2817	5.2804
	1	5.2528	5.2530	4.1517	4.1539	5.5782	5.5780	5.0641	5.0646	5.4271	5.4271
	2	5.3164	5.3169	4.1741	4.1769	5.6507	5.6509	5.1220	5.1228	5.4956	5.4960
	5	5.3968	5.3969	4.2209	4.2229	5.7391	5.7389	5.1975	5.1979	5.5804	5.5803
	8	5.4257	5.4254	4.2381	4.2393	5.7708	5.7702	5.2247	5.2246	5.6108	5.6103
	10	5.4358	5.4352	4.2432	4.2440	5.7821	5.7812	5.2341	5.2337	5.6216	5.6208

Table 4 Comparisons of the first three NDNFs of FG-CNTRC beams

(k_w, k_P)	V^*_{CNT}	Pattern	ω_{11}		ω_{22}		ω_{33}	
			(Yas and Samadi 2012)	Present	(Yas and Samadi 2012)	Present	(Yas and Samadi 2012)	Present
(0, .0)	0.12	UD	0.9753	0.9847	2.8728	2.8873	4.8704	4.8011
		FG-V	0.9453	0.8528	2.6424	2.6582	4.6675	4.5820
		FG-O	0.7527	0.7527	2.4562	2.4136	4.4320	4.2317
		FG-X	1.115	1.1295	3.0814	3.1048	5.0695	5.0100
	0.17	UD	1.1999	1.2119	3.6276	3.6424	6.2363	6.1346
		FG-V	1.1609	1.0413	3.3084	3.325	5.9498	5.8207
		FG-O	0.9155	0.9184	3.0577	3.0227	5.6139	5.4018
		FG-X	1.383	1.396	3.9293	3.9219	6.5447	6.3836
	0.28	UD	1.4401	1.457	4.1362	4.1508	6.9245	6.8099
		FG-V	1.4027	1.2651	3.8639	3.8583	6.7618	6.5672
		FG-O	1.1202	1.1289	3.6056	3.5951	6.4434	6.2742
		FG-X	1.6493	1.6429	4.4752	4.3462	7.3068	6.9165
(0.1, 0)	0.12	UD	1.0241	1.0329	2.8898	2.9036	4.8804	4.8103
		FG-V	0.9957	0.9081	2.6607	2.67602	4.6780	4.5918
		FG-O	0.815	0.8148	2.4760	2.4332	4.4430	4.2423
		FG-X	1.1581	1.1717	3.0972	3.1199	5.0791	5.0188
	0.17	UD	1.2396	1.2511	3.6409	3.6553	6.2441	6.1418
		FG-V	1.2019	1.0867	3.3229	3.3391	5.9579	5.8283
		FG-O	0.967	0.9696	3.0734	3.0382	5.6225	5.4101
		FG-X	1.4176	1.4302	3.9416	3.9338	6.5521	6.3904
	0.28	UD	1.4728	1.4892	4.1477	4.3567	6.9314	6.8162
		FG-V	1.4362	1.302	3.8762	3.8702	6.7688	6.5738
		FG-O	1.1619	1.1702	3.6187	3.6080	6.4508	6.2812
		FG-X	1.6779	1.6714	4.4858	4.3567	7.3133	6.9226
(0.1, 0.02)	0.12	UD	1.1144	1.1221	3.0203	3.0292	5.0552	4.9714
		FG-V	1.0883	1.0083	2.8013	2.8122	4.8596	4.7614
		FG-O	0.9258	0.9253	2.6268	2.5829	4.6338	4.4271
		FG-X	1.2386	1.251	3.2194	3.2365	5.2474	5.1719

Table 4 Continued

	0.17	UD	1.3145	1.3251	3.7444	3.7551	6.3804	6.2680
		FG-V	1.279	1.171	3.4354	3.4484	6.1002	5.9622
		FG-O	1.0612	1.0634	3.1951	3.1586	5.7731	5.5556
		FG-X	1.4836	1.4952	4.0375	4.0262	6.6822	6.5105
	0.28	UD	1.5352	1.5506	4.2372	4.2479	7.0523	6.9274
		FG-V	1.5002	1.3719	3.9714	3.9630	6.8923	6.6899
		FG-O	1.24	1.2476	3.7208	3.7078	6.5802	6.4041
		FG-X	1.733	1.7264	4.5688	4.4385	7.4280	7.0310

Table 5 Comparisons of the NDCBLs of FG-CNTRC beams

L/h	V_{CNT}^{*}	Reference	Pattern		
			UD	FG-X	FG-O
10	0.12	(Belarbi *et al*. 2023)	0.1655	0.2082	0.1049
		Present	0.1698	0.2078	0.1089
	0.17	(Belarbi *et al*. 2023)	0.2593	0.3260	0.1620
		Present	0.2664	0.3284	0.1679
	0.28	(Belarbi *et al*. 2023)	0.3584	0.4270	0.2414
		Present	0.3699	0.4319	0.2500
15	0.12	(Belarbi *et al*. 2023)	0.0988	0.1314	0.0574
		Present	0.1009	0.1329	0.0589
		(Yas and Samadi 2012)	0.0986	0.1288	0.0588
	0.17	(Belarbi *et al*. 2023)	0.1506	0.2011	0.0862
		Present	0.1541	0.2047	0.0884
		(Yas and Samadi 2012)	0.1505	0.1999	0.0877
	0.28	(Belarbi *et al*. 2023)	0.2206	0.2811	0.1324
		Present	0.2271	0.2891	0.1361
		(Yas and Samadi 2012)	0.2209	0.2896	0.1337
20	0.12	(Belarbi *et al*. 2023)	0.0630	0.0630	0.0351
		Present	0.0644	0.0884	0.0358
	0.17	(Belarbi *et al*. 2023)	0.0946	0.0946	0.0521
		Present	0.0970	0.1342	0.0532
	0.28	(Belarbi *et al*. 2023)	0.1430	0.1430	0.0812
		Present	0.1476	0.1981	0.0831
50	0.12	(Belarbi *et al*. 2023)	0.0119	0.0119	0.0062
		Present	0.0120	0.0136	0.0062
	0.17	(Belarbi *et al*. 2023)	0.0174	0.0174	0.0091
		Present	0.0178	0.0181	0.0092
	0.28	(Belarbi *et al*. 2023)	0.0276	0.0276	0.0144
		Present	0.0284	0.0285	0.0146

highest NDNFs, while FG-O consistently yields the lowest ones, irrespective of the volume fraction of CNTs. This trend persists across all vibration modes.

Example 4: In Table 5, the present results regarding non-dimensional critical buckling loads (NDCBLs) of the FG-CNTRC beams utilizing QUASI-3D HSDT versus different CNT configurations and *L/h* are compared with those of Belarbi *et al*. (2023) employing FE-HSDT and Yas and Samadi (2012) using DQM-TBT.

Example 5: Table 6 presents results regarding non-dimensional critical buckling loads (NDCBLs) of the FG-CNTRC beams utilizing quasi-3D HSDT versus different values of V_{CNT}^{*}, k_w and k_p are compared with those of (Yas and Samadi 2012) using DQM-TBT for *L/h*=15.

Table 6 Comparisons of the NDCBLs of FG-CNTRC beams

(k_w, k_P)	V^*_{CNT}	Reference	Pattern		
			UD	FG-X	FG-O
(0.1, 0)	0.12	(Yas and Samadi 2012)	0.108729	0.138965	0.068902
		Present	0.126061	0.168177	0.075192
	0.17	(Yas and Samadi 2012)	0.160697	0.210077	0.097836
		Present	0.164291	0.214886	0.098589
	0.28	(Yas and Samadi 2012)	0.231036	0.299774	0.143887
		Present	0.237288	0.299312	0.146326
(0.1, 0.02)	0.12	(Yas and Samadi 2012)	0.128729	0.158965	0.088903
		Present	0.131059	0.163051	0.089047
	0.17	(Yas and Samadi 2012)	0.180692	0.230077	0.117836
		Present	0.184291	0.234886	0.118589
		(Yas and Samadi 2012)	0.251036	0.319774	0.163887
		Present	0.257288	0.319312	0.166326

Table 7 First three NDNFs of FG-CNTRC beams having n-FGX distribution pattern

(k_w, k_P)	V^*_{CNT}	n	ω_{11}	ω_{22}	ω_{33}
(0, 0)	0.17	1	1.3960	3.9219	6.3836
		2	1.4823	4.0427	6.4909
		3	1.5339	4.1153	6.5568
		4	1.5691	4.1665	6.6047
		5	1.5950	4.2064	6.6436
(0.1, 0.02)		1	1.5109	4.0310	6.5132
		2	1.5909	4.1483	6.6178
		3	1.6391	4.2190	6.6820
		4	1.6720	4.2688	6.7286
		5	1.6963	4.3076	6.7667

Table 8 First three NDCBLs of FG-CNTRC beams having n-FGX distribution pattern

(k_w, k_P)	V^*_{CNT}	n	ω_{11}	ω_{22}	ω_{33}
(0, 0)	0.17	1	0.2047	0.4180	0.5254
		2	0.2309	0.4454	0.5462
		3	0.2474	0.4624	0.5593
		4	0.2589	0.4745	0.5689
		5	0.2676	0.4841	0.5768
(0.1, 0.02)		1	0.2398	0.4416	0.5470
		2	0.2660	0.4690	0.5678
		3	0.2824	0.4859	0.5809
		4	0.2940	0.4981	0.5905
		5	0.3026	0.5077	0.5983

Consequently, it is seen that the present results are in good agreement with the previously published ones, while the small discrepancies seem to arise from the applied numerical method.

4.2 Numerical Examples

Example 6: Tables 7 and 8 show the variations of NDFNFs and NDCBLs of FG-CNTRC beam for the n-FGX distribution pattern versus different exponent of the volume fraction of the CNTs n and a volume fraction of V^*_{CNT} with and without EFs for L/h=15. Table 7 demonstrates that the rise in NDNFs corresponds with an increase in the exponent of the CNT volume fraction. This finding is valid for the first three NDNFs, whether with or without foundation. The same behavior is recorded for the first three NDCBLs of FG-CNTRC beams as shown in Table 8.

Example 7: The variations of NDNFs of FG-CNTRC

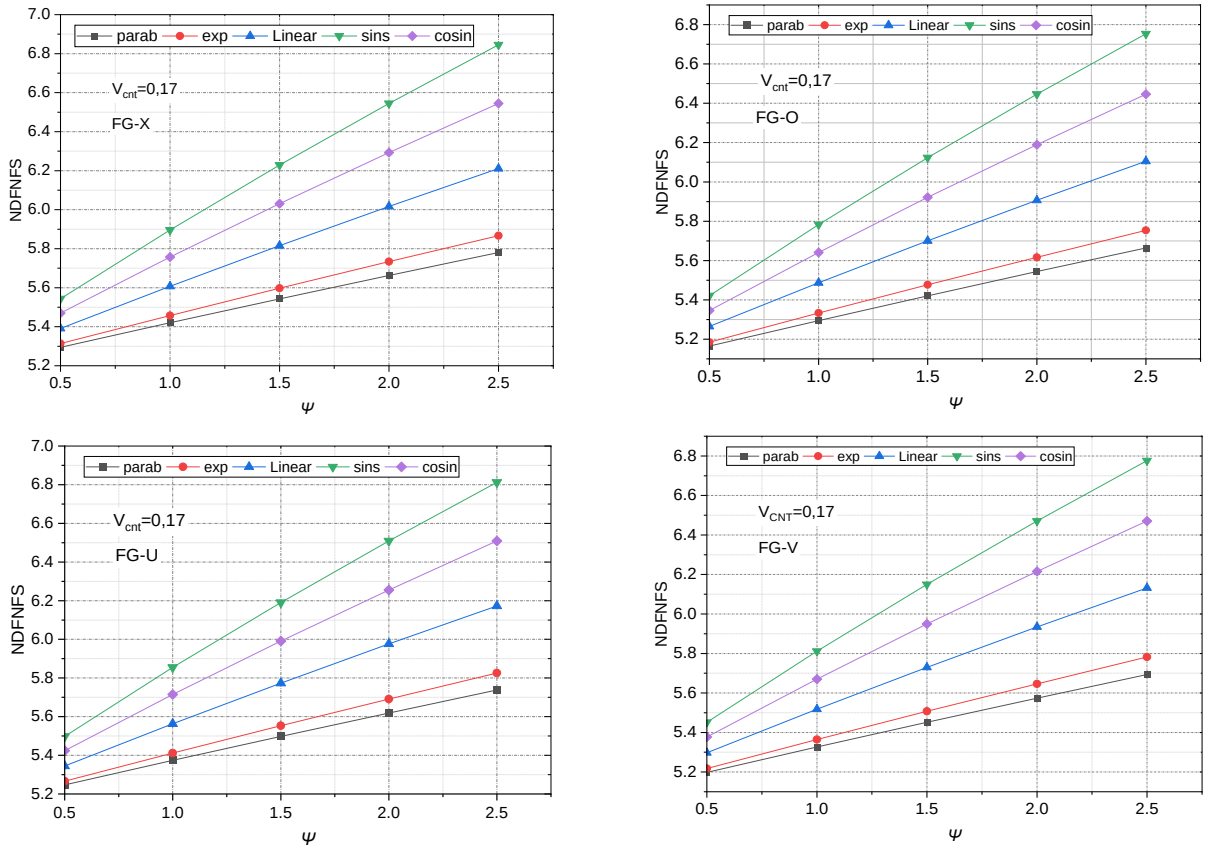

Fig. 2 The variation of NDFNFs of FG-CNTRC beams versus VEF coefficient ψ (V^*_{CNT}=0.17, L/h=10, k_w=10, k_p=1.5)

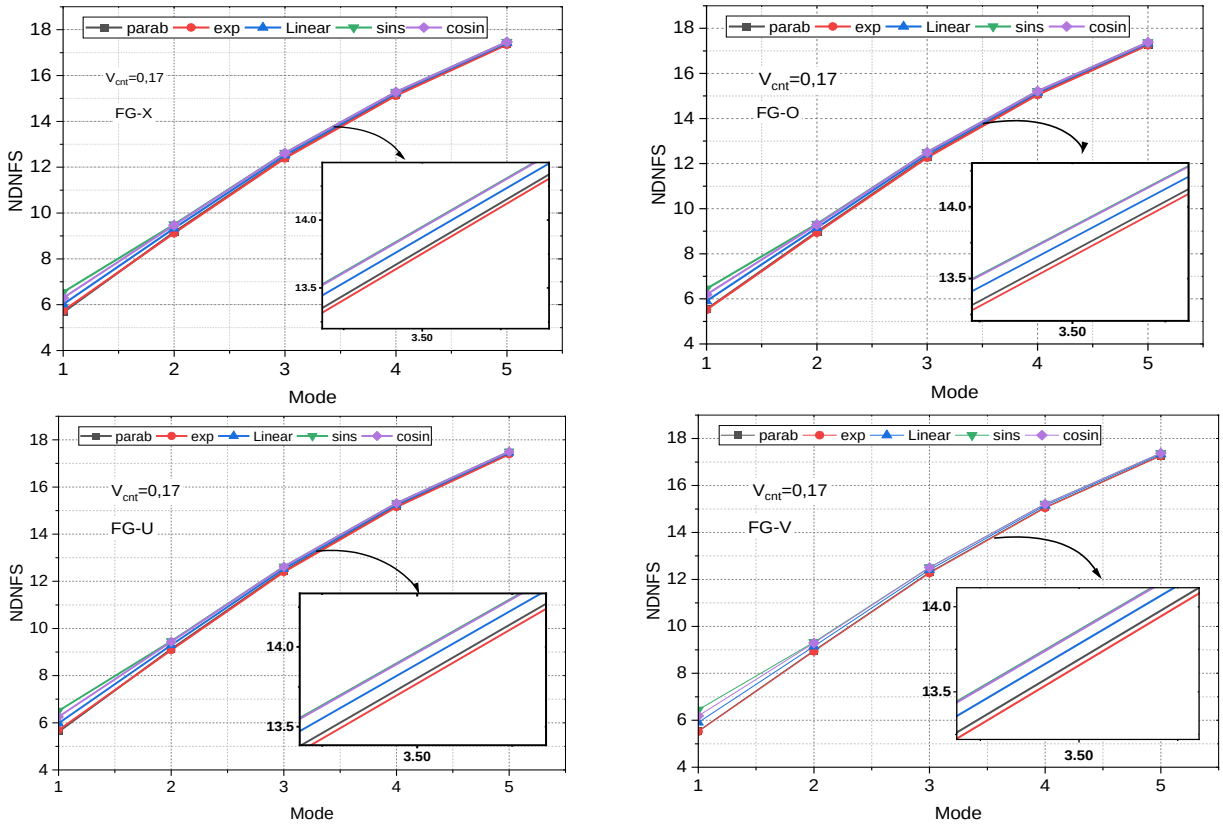

Fig. 3 The variation of NDNFs of FG-CNTRC beams versus the number of the mode (V^*_{CNT}=0.17, L/h=10, k_w=10, k_p=1.5. ψ=2)

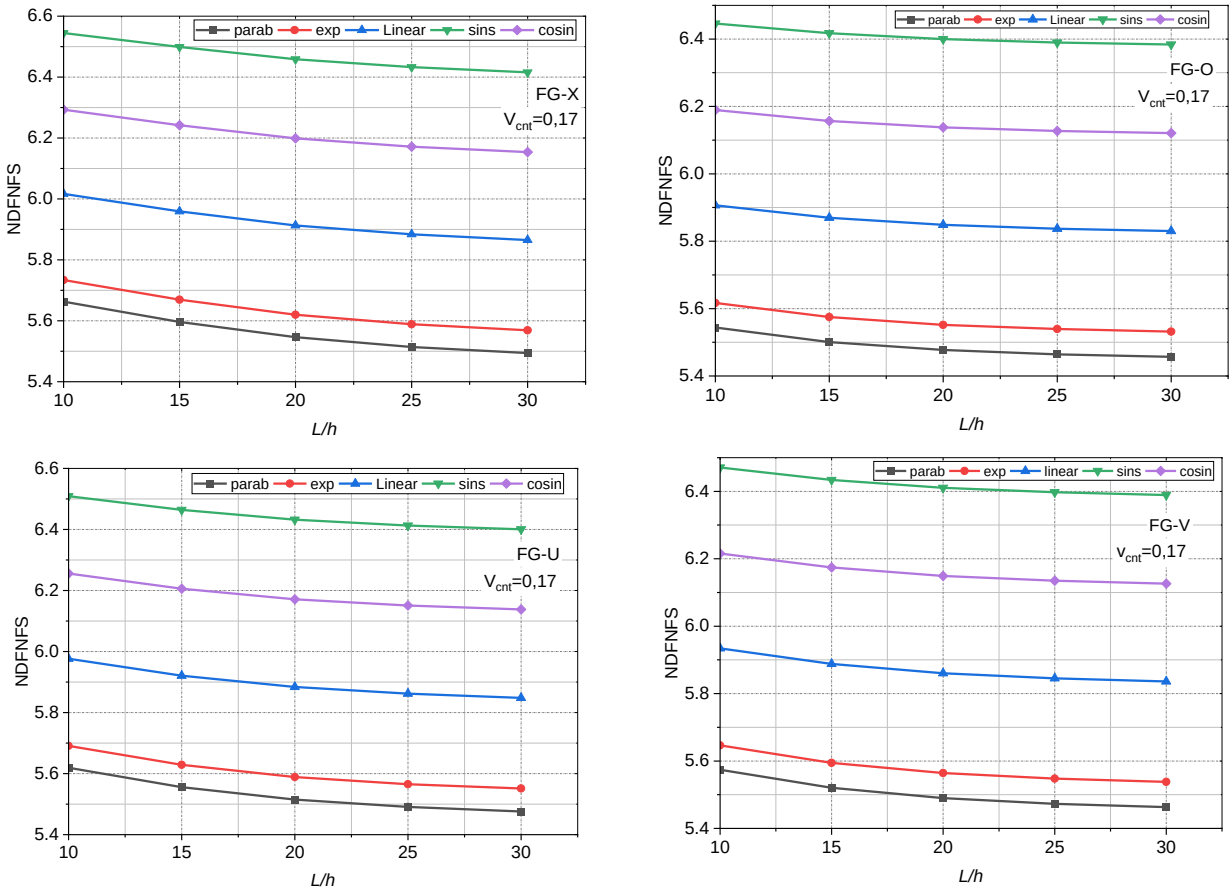

Fig. 4 The variation of NDFNFs of FG-CNTRC beams versus L/h (k_w=10, k_p=1.5, ψ=2)

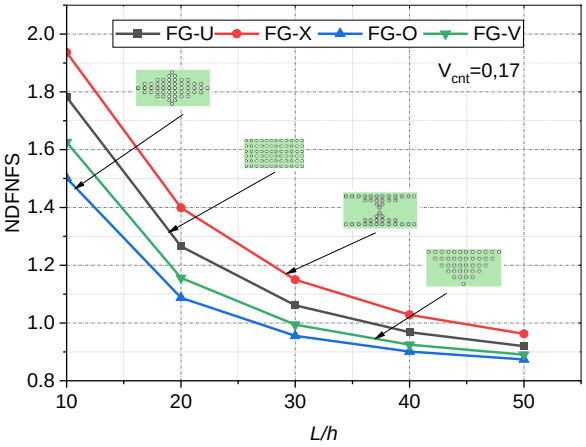

Fig. 5 The variation of NDFNFs of FG-CNTRC beams versus L/h (k_w=10, k_p=1.5. ψ=2).

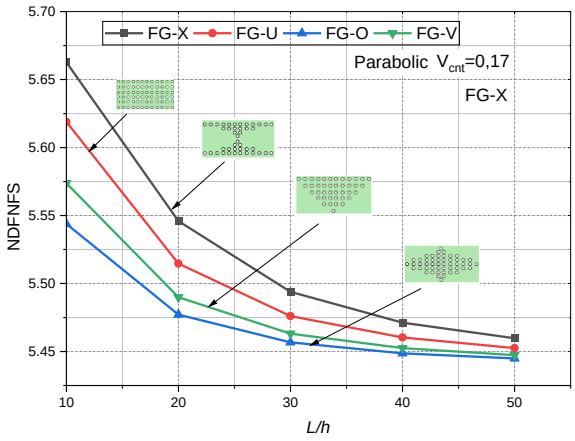

Fig. 6 The variation of NDFNFs of FG-CNTRC beams on VEFs versus L/h (k_w=10, k_p=1.5. ψ=2)

beams with FG-X, FG-O, UD, and FG-V CNT configurations on different kinds of VEFs are shown in Figs. 2-4. The variations are examined in relation to various vibration modes, the VEF coefficient (ψ), and the L/h. The NDFNFs grow in Fig. 2 with a greater coefficient ψ. In particular, the Winkler EF's sinusoidal variation yields the maximum frequency, whereas other EF variations result in a lower frequency. Variations in the distribution pattern of CNTs according to the mode can be observed in Fig. 3. NDNFs are higher because of the mode's amplification impact, regardless of the kind of foundation. It is remarkable that the NDNFs are not affected by changes in VEF. From Fig. 4, it is clear that NDFNFs fall with increasing L/h. Interestingly, the Winkler EF's sinusoidal variation produces the greatest NDFNF values; all other EF variations cause the NDFNF to fall.

Example 8: Fig. 5 shows the impact of the L/h on NDFNFs of FG-CNTRC beams. It is clear that when the L/h increases, the NDFNF falls, revealing a decrease in the stiffness of the FG-CNTRC beam. Interestingly, the FG-X

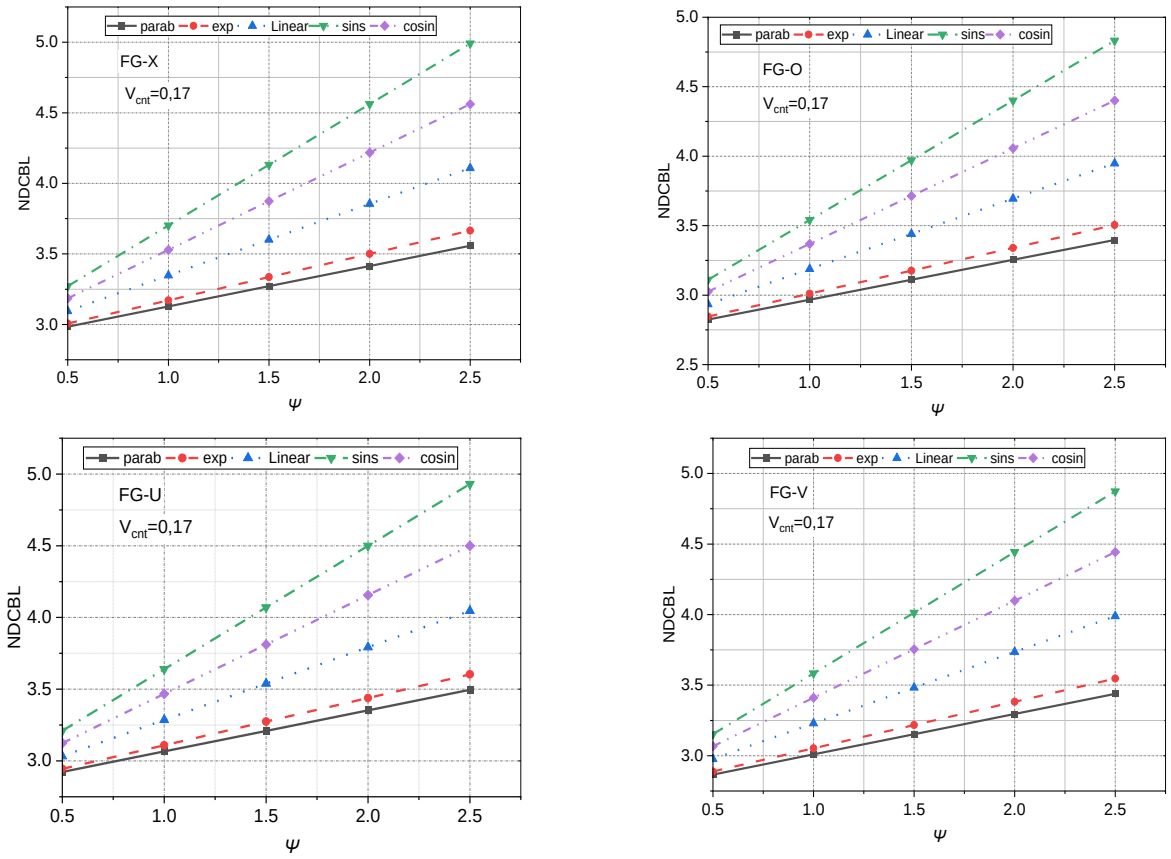

Fig. 7 The variation of NDCBLs of FG-CNTRC beams versus different VEF coefficients (V_{CNT}^{*}=0.17)

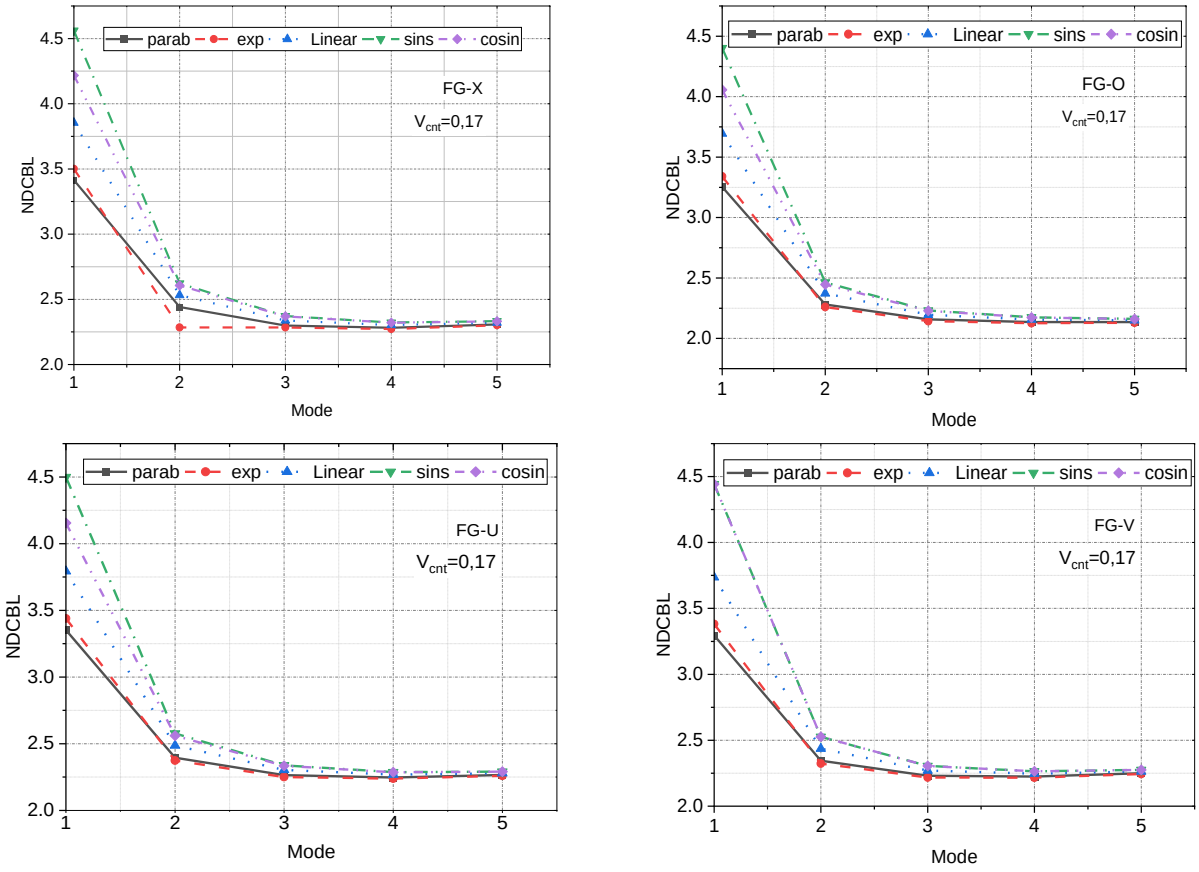

Fig. 8 The variation of NDCBLs of FG-CNTRC beams versus the number of the mode(V_{CNT}^{*}=0.17)

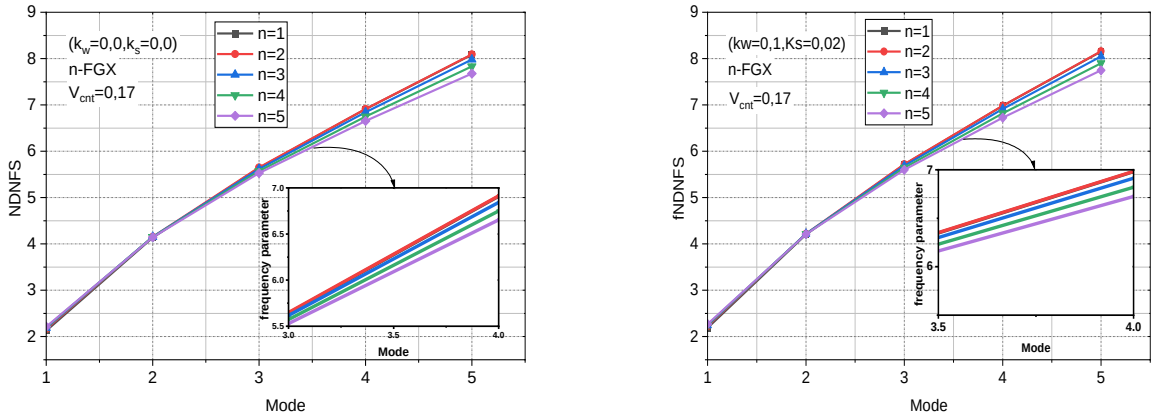

Fig. 9 The variation of NDNFs of FG-CNTRC having n-FGX distribution pattern with and without EF versus the number of modes

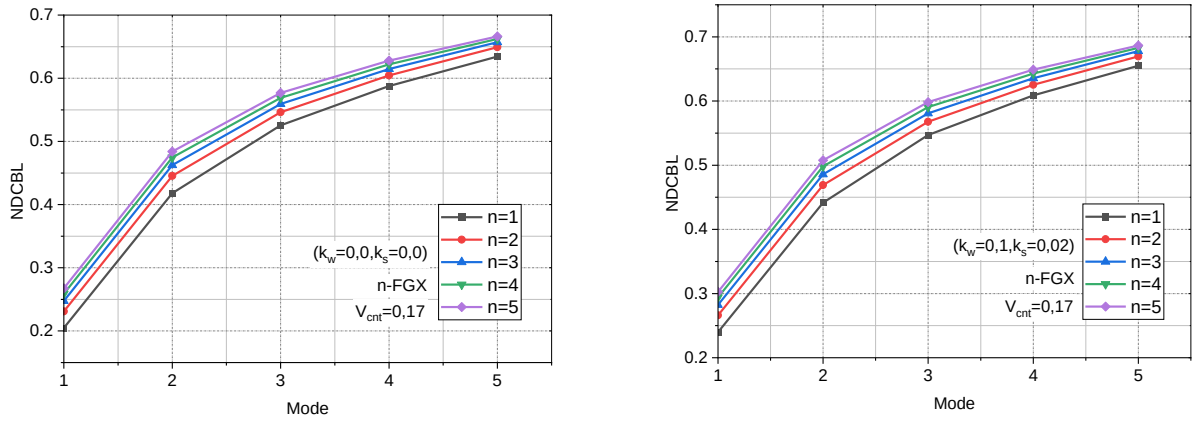

Fig. 10 The variation of NDCBLs of FG-CNTRC having n-FGX distribution pattern with and without EFs versus the number of the modes (V^*_{CNT}=0.17)

distribution pattern shows that the top and bottom surfaces have larger CNT concentrations, raising the NDFNF and improving resistance to bending by increasing stiffness in those areas and reducing it near the mid-plane. In contrast to the FG-X pattern's behavior, the FG-O pattern highlights the lowest NDFNF, implying that uniform and unsymmetrical distribution patterns of CNTs are less efficient in either raising or lowering the frequency than symmetric ones.

Example 9: Fig. 6 shows that as the *L/h* increases, the NDFNF of FG-CNTRC beams on EFs decreases. The FG-X distribution pattern has the greatest NDFNF values. Furthermore, the highest NDFNFs are linked to the Winkler EF in its parabolic form, depending on the kind of variation. Interestingly, in all other CNT distribution patterns, frequency is reduced.

Example 10: Fig. 7 illustrates those NDCBLs of the FG-CNTRC beam increase with a rise in the VEF coefficient ψ, taking into account four distribution patterns (FG-X, FG-O, FG-V, FG-U) of V^*_{CNT} with a volume fraction of 0.17, it is significant that the greatest NDCBL, is generated by the Winkler EF's sinusoidal change. Other EF changes, on the other hand, cause a decrease in NDCBL.

Example 11: It is clear from Fig. 8 that NDCBL diminishes as the number of the mode rises. Moreover, the sinusoidal variation of the Winkler EF shows the greatest NDCBL values. Notably, there is an alternating pattern of buckling rise and decrease between modes 2 and 3. Variations in the variation of Winkler EF do not affect the buckling, even when the number of the mode increases.

Example 12: Fig. 9 shows the variation of NDNFs of FG-CNTRC having n-FGX distribution pattern with and without EFs versus the number of the modes. for V^*_{CNT}=0.17. Because of the mode's amplification effect, the NDNFs are higher regardless of the number of modes. It can be concluded that the NDNFs increase with the increase in the number of modes.

Example 13: Fig. 10 illustrates the variation of the NDCBLs of FG-CNTRC having n-FGX distribution pattern with and without EFs versus the number of modes. It is clear that as the number of mode increases. It is clear that as the number of the mode increases the NDCBLs are also increase. The fifth mode produces the most significant NDCBL, in contrast to the other n values.

4. Conclusions

This study provides a comprehensive assessment of the influence of CNT distribution patterns, VEF types, and

length/thickness ratios on the mechanical behavior of FG-CNTRC beams, providing valuable information for optimizing structural performance. The present work examined the free vibration and buckling behaviours of FG-CNTRC beams on VEFs employing quasi-3D-HSDT. The rule of mixture was utilized to describe the effective material properties of FG-CNTRC beams. Different CNT distribution patterns were considered in this context. Hamilton's principle was used to derive the equations of motion, while Navier's method was used to solve the problem analytically.

Briefly, the following conclusions are drawn:

• With varying CNT distribution patterns, the values of NDNFs and NDCBLs of FG-CNTRC beams decrease as the length-to-thickness ratio increases.

• The volume fraction of CNTs significantly influences the NDNFs and NDCBLs of FG-CNTRC beams

• The type of VEF along the axial direction notably affects the NDNFs and NDCBLs of FG-CNTRC beams

• The sinusoidal type of the VEF and the FG-X distribution pattern with higher outer composition provide optimal values for both the NDNFs and NDCBLs of FG-CNTRC beams

• The values of NDNFs and NDCBLs of FG-CNTRC beam increase with the increment of mode and VEF coefficient

In future research, the influence of additional factors, such as temperature variations and material defects, on the mechanical behavior of FG-CNTRC beams will be investigated. Additionally, alternative nanofiller materials, such as graphene, will be explored to enhance the performance of various structural applications.

References

Abdelrahman, A.A., Esen, I., Tharwan, M.Y., Assie, A. and Eltaher, M.A. (2024), "On vibrations of functionally graded carbon nanotube (FGCNT) nanoplates under moving load", *Adv. Nano Res.*, **16**(4), 395-412. https://doi.org/10.12989/anr.2024.16.4.395.

Ait Atmane, H., Tounsi, A. and Bernard, F. (2017), "Effect of thickness stretching and porosity on mechanical response of a functionally graded beams resting on elastic foundations", *Int. J. Mech. Mater. Des*, **13**, 71-84. https://doi.org/10.1007/s10999-015-9318-x.

Alazwari, M.A., Daikh, A.A. and Eltaher, M.A. (2022), "Novel quasi 3D theory for mechanical responses of FG-CNTs reinforced composite nanoplates", *Adv. Nano Res.*, **12**(2), 117-137. https://doi.org/10.12989/anr.2022.12.2.117.

Alsubaie, A.M., Alfaqih, I., Al-Osta, M.A., Tounsi, A., Chikh, A., Mudhaffar, I.M. and Tahir, S. (2023), "Porosity-dependent vibration investigation of functionally graded carbon nanotube-reinforced composite beam", *Comput. Concr.*, **32**(1), 75-85. https://doi.org/10.12989/cac.2023.32.1.075

Alsubaie, A.M., Al-Osta, M.A., Alfaqih, I., Tounsi, A., Chikh, A., Mudhaffar, I.M., Al-Dulaijan, S.U. and Tahir, S. (2024), "Influences of porosity distributions on bending and buckling behaviour of functionally graded carbon nanotube-reinforced composite beam", *Comput. Concr.*, **34**(2), 179-193. https://doi.org/10.12989/cac.2024.34.2.179

Avcar, M., Hadji, L. and Akan, R. (2022), "The influence of Winkler-Pasternak elastic foundations on the natural frequencies of imperfect functionally graded sandwich beams", *Geomech. Eng.*, **31**(1), 99-112. https://doi.org/10.12989/gae.2022.31.1.099.

Avcar, M., Hadji, L. and Civalek, Ö. (2023), "The influence of non-linear carbon nanotube reinforcement on the natural frequencies of composite beams", *Adv. Nano Res.*, **14**(5), 421-433. https://doi.org/10.12989/anr.2023.14.5.421.

Babaei, H., Kiani, Y. and Reza Eslami, M. (2021), "Perturbation method for thermal post-buckling analysis of shear deformable FG-CNTRC beams with different boundary conditions", *Int. J. Struct. Stab. Dyn.*, **21**(13). https://doi.org/10.1142/S0219455421501753.

Beitollahi, A., Janghorban, M., Bazargan-Lari, Y. and Tounsi, A. (2025), "On the variable length scale parameter for agglomeration of nanoparticles in nanocomposites", *Proceedings of the Institution of Mechanical Engineers, Part C: Journal of Mechanical Engineering Science*, 2025. https://doi.org/10.1177/09544062241308513

Belarbi, M.O., Salami, S.J., Garg, A., Daikh, A.A., Houari, M.S.A., Dimitri, R. and Tornabene, F. (2023), "Mechanical behavior analysis of FG-CNT-reinforced polymer composite beams via a hyperbolic shear deformation theory", *Contin. Mech. Thermodyn.*, **35**(2), 497-520. https://doi.org/10.1007/s00161-023-01191-2.

Bhangale, R.K. and Ganesan, N. (2006), "Free vibration of functionally graded non-homogeneous magneto-electro-elastic cylindrical shell", *Int. J. Comput. Meth. Eng. Sci. Mech.*, **7**(3), 191-200. https://doi.org/10.1080/15502280500388102.

Chen, W.Q., Lü, C.F. and Bian, Z.G. (2004), "A mixed method for bending and free vibration of beams resting on a Pasternak elastic foundation", *Appl. Math. Model.*, **28**(10), 877-890. https://doi.org/10.1016/j.apm.2004.04.001.

Cheshmeh, E., Karbon, M., Eyvazian, A., Jung, D.W., Habibi, M. and Safarpour, M. (2022), "Buckling and vibration analysis of FG-CNTRC plate subjected to thermo-mechanical load based on higher order shear deformation theory", *Mech. Based Des. Struct. Mach.*, **50**(4), 1137-1160. https://doi.org/10.1080/15397734.2020.1744005.

Civalek, Ö., Dastjerdi, S. and Akgöz, B. (2022), "Buckling and free vibrations of CNT-reinforced cross-ply laminated composite plates", *Mech. Based Des. Struct. Mach.*, **50**(6), 1914-1931. https://doi.org/10.1080/15397734.2020.1766494.

Cuong, B.M., Tounsi, A., Thom, D.V., Hai Van, N.T. and Minh, P.V. (2024), "Finite element modelling for the static bending response of rotating FG-GPLRC beams with geometrical imperfections in thermal mediums", *Comput. Concr.*, **33**(1), 91-102. https://doi.org/10.12989/cac.2024.33.1.091

Eghbali, M. and Hosseini, S.A. (2024), "An accurate analytical exploration for dynamic response of thermo-electric CNTRC beams under driving harmonic and constant loads resting on Pasternak foundation", *Adv. Nano Res.*, **16**(6), 549-564. https://doi.org/10.12989/anr.2024.16.6.549.

El-Ashmawy, A.M. and Xu, Y. (2021), "Combined effect of carbon nanotubes distribution and orientation on functionally graded nanocomposite beams using finite element analysis", *Mater. Res. Express*, **8**(1). https://doi.org/10.1088/2053-1591/abc773.

Fallah, A., Botshekanan Dehkordi, M., Nourbakhsh, H. and Tadi Beni, Y. (2021), "Semi-exact solution for non-linear dynamic analysis of graded carbon nanotube-reinforced beam with graded shape memory wires", *Mech. Adv. Mater. Struct.*, **28**(6), 568-582. https://doi.org/10.1080/15376494.2019.1578012.

Ferreira, A.J.M., Batra, R.C., Roque, C.M.C., Qian, L.F. and Martins, P.A.L.S. (2005), "Static analysis of functionally graded plates using third-order shear deformation theory and a meshless method", *Compos. Struct.*, **69**(4), 449-457. https://doi.org/10.1016/j.compstruct.2004.08.003.

Gawah, Q., Al-Osta, M.A., Bourada, F., Tounsi, A., Ahmad, S. and Al-Zahrani, M.M. (2025), "Bending analysis of graphene

platelet-reinforced FG plates on Kerr foundations using an integral HSDT", *Acta Mech*., 1-25. https://doi.org/10.1007/s00707-025-04236-6

Ghasemi, A.R., Mohandes, M., Dimitri, R. and Tornabene, F. (2019), "Agglomeration effects on the vibrations of CNTs/fiber/polymer/metal hybrid laminates cylindrical shell", *Compos. B Eng*., **167**, 700-716. https://doi.org/10.1016/j.compositesb.2019.03.028.

Ghorbani Shenas, A., Ziaee, S. and Malekzadeh, P. (2019), "A unified higher-order beam theory for free vibration and buckling of fgcnt-reinforced microbeams embedded in elastic medium based on unifying stress–strain gradient framework", *Iran. J. Sci. Technol. Trans. Mech. Eng*., **43**, 469-492. https://doi.org/10.1007/s40997-018-0171-z.

Golmakani, M.E. and Zeighami, V. (2018), "Nonlinear thermo-elastic bending of functionally graded carbon nanotube-reinforced composite plates resting on elastic foundations by dynamic relaxation method", *Mech. Adv. Mater. Struct*., **25**(10), 868-880. https://doi.org/10.1080/15376494.2017.1310336.

Golmakani, M.E., Esmaeilzadeh, M., Sadeghian, M. and Zeighami, V. (2021), "Buckling analysis of CNTRC plates in the thermal environment based on combination of the incremental load technique and dynamic relaxation method", *Int. J. Comput. Meth. Eng. Sci. Mech*., **22**(4), 316-332. https://doi.org/10.1080/15502287.2021.1882615.

Han, Y. and Elliott, J. (2007), "Molecular dynamics simulations of the elastic properties of polymer/carbon nanotube composites", *Comput. Mater. Sci*., **39**(2), 315-323. https://doi.org/10.1016/j.commatsci.2006.06.011.

Hetényi, M. and Hetbenyi, M.I. (1946), *Beams On Elastic Foundation: Theory with Applications In The Fields Of Civil and Mechanical Engineering*, **16**, Ann Arbor, MI: University of Michigan Press, U.S.A.

Hussain, M., Khadimallah, M.A., Ayed, H., Ghandourah, E., Mouldi, A. and Tounsi, A. (2024), "Closed form interaction for safety assessment of DWCNTs: Mechanical vibration", *Adv. Nano Res*., **17**(4), 315-321. https://doi.org/10.12989/anr.2024.17.4.315.

Iijima, S. (1991), "Helical microtubules of graphitic carbon", *Nature*, **354**, 56-58. https://doi.org/10.1038/354056a0.

Khelifa, Z., Hadji, L., Daouadji, T.H. and Bourada, M. (2018), "Buckling response with stretching effect of carbon nanotube-reinforced composite beams resting on elastic foundation", *Struct. Eng. Mech*., **67**(2), 125-130. https://doi.org/10.12989/sem.2018.67.2.125.

Kiarasi, F., Asadi, A., Babaei, M., Asemi, K. and Hosseini, M. (2022), "Dynamic analysis of functionally graded carbon nanotube (FGCNT) reinforced composite beam resting on viscoelastic foundation subjected to impulsive loading", *J. Comput. Appl. Mech*., **53**(1), 1-23. https://doi.org/10.22059/jcamech.2022.339008.693.

Lin, F. and Xiang, Y. (2014). "Vibration of carbon nanotube reinforced composite beams based on the first and third order beam theories", *Appl. Math. Model*., **38**(15-16), 3741-3754. https://doi.org/10.1016/j.apm.2014.02.008.

Mellal, F., Bennai, R., Avcar, M., Nebab, M. and Atmane, H.A. (2023), "On the vibration and buckling behaviors of porous FG beams resting on variable elastic foundation utilizing higher-order shear deformation theory", *Acta Mech*., **234**(9), 3955-3977. https://doi.org/10.1007/s00707-023-03603-5.

Mellal, F., Bennai, R., Nebab, M., Atmane, H. A., Bourada, F., Hussain, M. and Tounsi, A. (2024), "Investigation on the effect of porosity on wave propagation in FGM plates resting on elastic foundations via a quasi-3D HSDT", *Waves Random Complex Med*. **34**(5), 3727-3753. https://doi.org/10.1080/17455030.2021.1983235.

Mohammadimehr, M., Mohammadi-Dehabadi, A.A., Alavi, S.A., Alambeigi, K., Bamdad, M., Yazdani, R. and Hanifehlou, S. (2018), "Bending, buckling, and free vibration analyses of carbon nanotube reinforced composite beams and experimental tensile test to obtain the mechanical properties of nano-composite", *Steel Compos. Struct*., **29**(3), 405-422. https://doi.org/10.12989/scs.2018.29.3.405.

Mohseni, A. and Shakouri, M. (2019), "Vibration and stability analysis of functionally graded CNT-reinforced composite beams with variable thickness on elastic foundation", *Proc. Inst. Mech. Eng. L: J. Mater.: Des. Appl*., **233**(12), 2478-2489. https://doi.org/10.1177/1464420719866222.

Nampally, P., Ruocco, E. and Reddy, J.N. (2021). "Bending analysis of functionally graded rectangular plates using the dual mesh control domain method", *Int. J. Comput. Meth. Eng. Sci. Mech*., **22**(5), 425-437. https://doi.org/10.1080/15502287.2021.1890279.

Nebab, M., Atmane, H.A., Bennai, R. and Tounsi, A. (2019a), "Effect of variable elastic foundations on static behavior of functionally graded plates using sinusoidal shear deformation", *Arab. J. Geosci*., **12**(24), 809. https://doi.org/10.1007/s12517-019-4871-5.

Nebab, M., Atmane, H.A., Bennai, R. and Tahar, B. (2019b), "Effect of nonlinear elastic foundations on dynamic behavior of FG plates using four-unknown plate theory", *Earthq. Struct*., **17**(5), 447-462. https://doi.org/10.12989/eas.2019.17.5.447.

Nebab, M., Atmane, H.A., Bennai, R., Tounsi, A. and Bedia, E.A. (2019c), "Vibration response and wave propagation in FG plates resting on elastic foundations using HSDT", *Struct. Eng. Mech*., **69**(5), 511-525. https://doi.org/10.12989/sem.2019.69.5.511.

Peng, X., Xu, J., Yang, E., Li, Y. and Yang, J. (2022), "Influence of the boundary relaxation on free vibration of functionally graded carbon nanotube-reinforced composite beams with geometric imperfections", *Acta Mech*., **233**(10), 4161-4177. https://doi.org/10.1007/s00707-022-03320-5.

Ranjbar, M. and Feli, S. (2019), "Temperature-dependent analysis of axially functionally graded CNT reinforced micro-cantilever beams subjected to low velocity impact", *Mech. Adv. Mater. Struct*., **26**(13), 1154-1168. https://doi.org/10.1080/15376494.2018.1432788.

Sekkak, M., Zerrouki, R., Zidour, M., Tounsi, A., Bourada, M., Selim, M.M. and Saad, H.A. (2024), "Static analysis of nonlinear FG-CNT reinforced nano-composite beam resting on Winkler/Pasternak foundation", *Adv. Nano Res*., **16**(5), 509-519. https://doi.org/10.12989/anr.2024.16.5.509.

Selvadurai, A.P. (2013), *Elastic Analysis of Soil-Foundation Interaction*, Elsevier.

Shen, H.S. (2009), "Nonlinear bending of functionally graded carbon nanotube-reinforced composite plates in thermal environments", *Compos. Struct*., **91**(1), 9-19. https://doi.org/10.1016/j.compstruct.2009.04.026.

Shi, Z., Yao, X., Pang, F. and Wang, Q. (2017), "An exact solution for the free-vibration analysis of functionally graded carbon-nanotube-reinforced composite beams with arbitrary boundary conditions", *Sci. Rep*., **7**(1). https://doi.org/10.1038/s41598-017-12596-w.

Sobhani, E. and Avcar, M. (2022), "The influence of various nanofiller materials (CNTs, GNPs, and GOPs) on the natural frequencies of nanocomposite cylindrical shells: A comparative study", *Mater. Today Commun*., **33**. https://doi.org/10.1016/j.mtcomm.2022.104547.

Taati, E., Borjalilou, V., Fallah, F. and Ahmadian, M.T. (2022), "On size-dependent nonlinear free vibration of carbon nanotube-reinforced beams based on the nonlocal elasticity theory: Perturbation technique", *Mech. Based Des. Struct. Mach*., **50**(6), 2124-2146. https://doi.org/10.1080/15397734.2020.1772087.

Thostenson, E.T., Ren, Z. and Chou, T.W. (2001), "Advances in the science and technology of carbon nanotubes and their

composites: A review", *Compos. Sci. Technol*., **61**(13), 1899-1912. https://doi.org/10.1016/S0266-3538(01)00094-X.

Tlidji, Y., Zidour, M., Zerrouki, R., Benahmed, A., Serbah, B., Draiche, K. and Bouakkaz, K. (2024), "Nonlinear FG-CNT effect on the critical buckling load of nanocomposite beams with different boundary conditions", *Adv. Nano Res*., **17**(4), 323-334. https://doi.org/10.12989/anr.2024.17.4.323.

Tornabene, F., Fantuzzi, N., Bacciocchi, M. and Viola, E. (2016), "Effect of agglomeration on the natural frequencies of functionally graded carbon nanotube-reinforced laminated composite doubly-curved shells", *Compos. B: Eng*., **89**, 187-218. https://doi.org/10.1016/j.compositesb.2015.11.016.

Wang, Z.X. and Shen, H.S. (2012), "Nonlinear vibration and bending of sandwich plates with nanotube-reinforced composite face sheets", *Compos. B: Eng*., **43**(2), 411-421. https://doi.org/10.1016/j.compositesb.2011.04.040.

Wu, H.L., Yang, J. and Kitipornchai, S. (2016), "Nonlinear vibration of functionally graded carbon nanotube-reinforced composite beams with geometric imperfections", *Compos. B Eng*., **90**, 86-96. https://doi.org/10.1016/j.compositesb.2015.12.007.

Yas, M.H. and Samadi, N. (2012), "Free vibrations and buckling analysis of carbon nanotube-reinforced composite Timoshenko beams on elastic foundation", *Int. J. Press. Vessels Pip*., **98**, 119-128. https://doi.org/10.1016/j.ijpvp.2012.07.012.

Youzera, H., Meftah, S.A., Tounsi, A., Salem, M.A., Khedher, K. M. and Yaylacı, M.(2025), "Free vibration analysis of sandwich cylindrical shells with functionally graded carbon nanotube-reinforced composite face sheets using the differential quadrature (DQ) method", *Acta Mech*., 1-16. https://doi.org/10.1007/s00707-025-04230-y

Ying, J., Lü, C.F., and Chen, W.Q. (2008), "Two-dimensional elasticity solutions for functionally graded beams resting on elastic foundations", *Compos. Struct*., **84**(3), 209-219. https://doi.org/10.1016/j.compstruct.2007.07.004.

Yuan, Y., Niu, Z. and Smitt, J. (2023), "Magneto-hygro-thermal vibration analysis of the viscoelastic nanobeams reinforcedwith carbon nanotubes resting on Kerr's elastic foundation based on NSGT", *Adv. Compos. Mater*., **32**(4), 568-590. https://doi.org/10.1080/09243046.2022.2122766.

Zeighami, V., Jafari, M. and Jafari, M. (2023), "Using Laurent's series in the theoretical solution to estimate the stress resultants of FG-CNTRC plates weakened by a central cutout at different temperatures", *Int. J. Comput. Meth. Eng. Sci. Mech*., **24**(4), 227-246. https://doi.org/10.1080/15502287.2022.2150721.

Zerrouki, R., Karas, A. and Zidour, M. (2020), "Critical buckling analyses of nonlinear FG-CNT reinforced nano-composite beam", *Adv. Nano Res*., **9**(3), 211-220. https://doi.org/10.12989/anr.2020.9.3.211.

Zhang, H., Gao, C., Li, H., Pang, F., Zou, T., Wang, H. and Wang, N. (2020), "Analysis of functionally graded carbon nanotube-reinforced composite structures: a review", *Nanotechnol. Rev*., **9**(1), 1408-1426. https://doi.org/10.1515/ntrev-2020-0110.

Zhang, Y.W., Ding, H.X., She, G.L. and Tounsi, A. (2023), "Wave propagation of CNTRC beams resting on elastic foundation based on various higher-order beam theories", *Geomech. Eng*., **33**(4), 381-391. https://doi.org/10.12989/gae.2023.33.4.381

CC